



**CHALMERS**  
UNIVERSITY OF TECHNOLOGY

## **Strong Electron Self-Cooling in the Cold-Electron Bolometers Designed for CMB Measurements**

Downloaded from: <https://research.chalmers.se>, 2024-04-18 21:44 UTC

Citation for the original published paper (version of record):

Kuzmin, L., Pankratov, A., Gordeeva, A. et al (2018). Strong Electron Self-Cooling in the Cold-Electron Bolometers Designed for CMB Measurements. Journal of Physics: Conference Series, 969(1). <http://dx.doi.org/10.1088/1742-6596/969/1/012069>

N.B. When citing this work, cite the original published paper.

# Strong Electron Self-Cooling in the Cold-Electron Bolometers Designed for CMB Measurements

L.S. Kuzmin<sup>\*,1,2</sup>, A.L. Pankratov<sup>2</sup>, A.V. Gordeeva<sup>2</sup>, V.O. Zbrozhek<sup>2</sup>, L.S. Revin<sup>2</sup>, V.A. Shamporov<sup>1,2</sup>, S. Masi<sup>3</sup> and P. de Bernardis<sup>3</sup>

<sup>1</sup>Chalmers University of Technology, Gothenburg, Sweden,

<sup>2</sup>Nizhny Novgorod State Technical University, Nizhnij Novgorod, Russia,

<sup>3</sup>Sapienza University of Rome, Italy

\*[kuzmin@chalmers.se](mailto:kuzmin@chalmers.se)

**Abstract.** We have realized cold-electron bolometers (CEB) with direct electron self-cooling of the nanoabsorber by SIN (Superconductor-Insulator-Normal metal) tunnel junctions. This electron self-cooling acts as a strong negative electrothermal feedback, improving noise and dynamic properties. Due to this cooling the photon-noise-limited operation of CEBs was realized in array of bolometers developed for the 345 GHz channel of the OLIMPO Balloon Telescope in the power range from 10 pW to 20 pW at phonon temperature  $T_{ph}=310$  mK. The negative electrothermal feedback in CEB is analogous to TES but instead of artificial heating we use cooling of the absorber. The high efficiency of the electron self-cooling to  $T_e=100$  mK without power load and to  $T_e=160$  mK under power load is achieved by:

- a very small volume of the nanoabsorber ( $0.02 \mu\text{m}^3$ ) and a large area of the SIN tunnel junctions,
- effective removal of hot quasiparticles by arranging double stock at both sides of the junctions and close position of the normal metal traps,
- self-protection of the 2D array of CEBs against interferences by dividing them between N series CEBs (for voltage interferences) and M parallel CEBs (for current interferences),
- suppression of Andreev reflection by a thin layer of Fe in the AlFe absorber.

As a result even under high power load the CEBs are working at electron temperature  $T_e$  less than  $T_{ph}$ . To our knowledge, there is no analogue in the bolometers technology in the world for bolometers working at electron temperature colder than phonon temperature.

## 1. Introduction

Cosmic microwave background (CMB) measurements were ranked second by the journal Science among the top 10 Achievements of the Decade [1]. Starting with the BOOMERanG experiment [2], increasing precision maps of the CMB have been obtained, with improved sky and frequency coverage. These measurements culminated with the all-sky multi-frequency maps of the WMAP and Planck satellites, and the high resolution maps of the SPT and ACT telescopes. The current trend of CMB measurements focuses on polarization measurements (see e.g. the BICEP/Keck measurements) and on the measurement of the Sunyaev-Zeldovich effect (carried out with ground based telescopes like SPT and ACT, and multifrequency space missions like the Planck satellite). The OLIMPO experiment [3] is a mm-wave balloon-borne telescope, optimized for spectral measurements of the Sunyaev-Zeldovich effect (the distortion of the spectrum of the CMB in the direction of rich galaxy clusters) within four frequency bands: 150, 210, 345 and 480 GHz. The power of spectral measurements of the SZ effect is to solve the degeneracies between different sources of signals along the line of sight, as described in [4].



We have realized the photon-noise-limited 2D array of cold electron bolometers (CEB) [5-7] for the 345 GHz band of the OLIMPO, based on the strong direct electron self-cooling of the nanoabsorbers by SIN tunnel junctions of the CEBs (Fig. 1). The electron cooling is based on decoupling of electron and phonon systems at low temperatures [8]. This effect was observed for the first time in a SIN tunnel junction by Nahum et al. [9]. Then the cooling effect in a single SIN junction was demonstrated in several laboratories from 300 to 100 mK [10,11].

After that, the efforts were mainly directed towards the development of micro-refrigerators based on cooling platform [12-14] with the potential of cooling a bolometer in thermal contact with the platform at lower temperature down to 100 mK. However, this strategy of indirect cooling met severe problems related with creation of suspended membrane and cooling through two very weak electron-phonon (e-ph) and phonon-electron (ph-e) coupling. Practically speaking, creation of bolometers on cooling platform failed after 20 years of development [15]. Cooling of platform itself was realized only from 300 to 200 mK and no one bolometer was placed so far on the platform for testing [15].

On the contrary, we have avoided all these problems by developing a competing concept of CEB with direct electron self-cooling of the absorber by SIN junctions [5,6]. Coupling of external radiation is realized through capacitance of the tunnel junctions [6,16]. Electron cooling is serving as strong electrothermal feedback as in TES [6,17] but with principle difference: artificial heating of TES is replaced by strong electron cooling.

The high efficiency of electron cooling ( $P_{cool}/IV = 40\%$ ) is achieved by the combination of the factors:

- a very small volume of the absorber ( $0.02 \mu\text{m}^3$ ) and a large relative area of tunnel junctions (80% of an area of the absorber  $S=1.6 \mu\text{m}^2$ ),
- effective removing of hot quasiparticles by double stock of them to superconducting external electrodes at both ends of the tunnel junctions,
- close position of the normal metal traps to SIN junctions at  $1.6 \mu\text{m}$  to catch hot quasiparticles and remove them from tunnel junction to avoid recombination of them and back heating of the absorber.
- self-protection of the 2D array of CEBs against interferences by dividing them between N\*M bolometers (N - series and M - parallel connections). For presented array  $N=48$  and  $M=4$  (Fig. 2),
- avoiding additional heating of the absorber by suppression of Andreev reflection by thin layer of Fe in AlFe absorber.

The structure is designed for the following requirements: bandwidth  $\Delta\nu = (330-360)$  GHz, sensitive to dual polarizations, power load from 20 to 90 pW (33 pW in photometer mode, 66 pW in spectrometer mode, 1.5 coefficient for margins), absorption efficiency not less than 50%, bolometer noise equivalent power  $NEP_{CEB}$  is less than photon noise equivalent power  $NEP_{phot}$ , where  $NEP_{phot}^2 = 2h\nu P_0 + P_0^2/\Delta\nu$ .

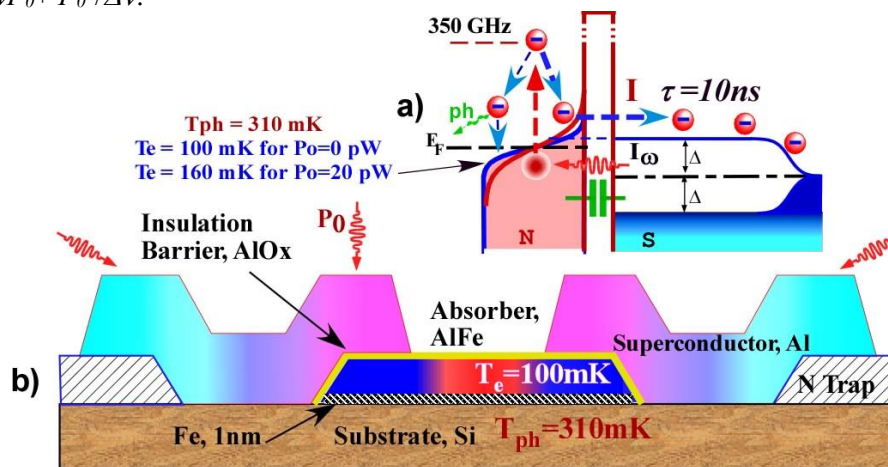


Fig. 1. a) Energy diagram of a CEB including normal absorber, isolation barrier and superconducting electrode, b) Cross-section of the CEB comprising two SIN tunnel junctions, an absorber and normal metal traps. The CEB demonstrates strong electron self-cooling from 310 mK to 100 mK providing perfect noise performance.

This paper is devoted to practical development of 2D arrays of CEBs for realization of photon-noise limited operation with bandwidth and efficiency required for OLIMPO Balloon Telescope. The comprehensive theoretical description can be found in [16], [18] and [19].

## 2. Array of CEBs in Current-Biased Mode.

Theoretical analysis has shown that 10% bandwidth can be achieved in the 2D array of CEBs [18] realized as meander-type structure [19] shown in Fig. 2. The geometry of the unit cell is created from the dense rectangular grid in a way that makes more uniform sparse distribution of dipoles over the unit cell. All CEBs are connected in series and parallel at DC for optimal matching with a JFET amplifier AD745 [20]. A pair of  $\lambda/2$  dipoles with wide electrodes sensitive to the both orthogonal linear polarizations is connected to another pair by high-inductive  $1\ \mu\text{m}$  wide lines. The impedance of each bolometer was determined by  $50\ \Omega$  resistance in series with  $20\ \text{fF}$  capacitance. The layout dimensions are optimized for the frequency band of 330-360 GHz, determined by band-pass filters.

The design of the pixel has started from the constructing of a numerical model and calculation of the absorption efficiency. The model consists of a horn, waveguide port, Si substrate, CEBs array with gold antennas and metallic backshort (Fig. 2). The thickness of the substrate and distance to the backshort are optimized to get maximal absorption at 345 GHz and to avoid excitation of substrate modes. The total number of bolometers and serial-parallel DC-connections had been determined by numerical simulations of the heat balance equations and in order to cover the most of the Airy disc increasing in this way the total absorbed power.

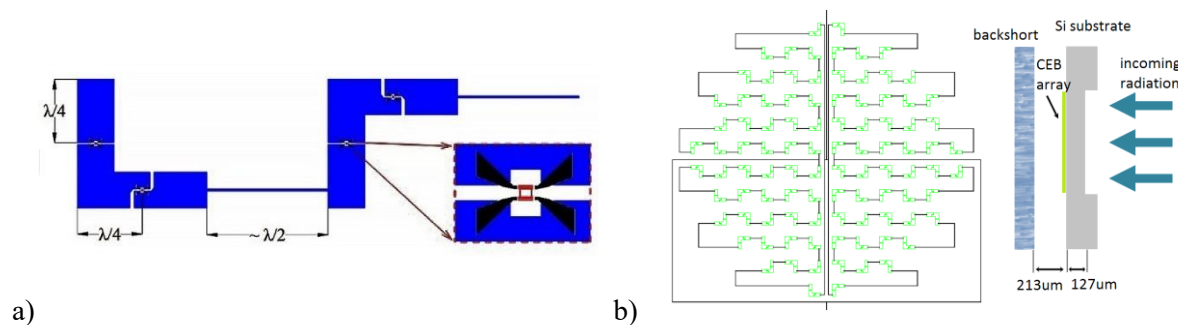


Fig. 2. a) Meander structure of 2D array of  $\lambda/2$  dipoles with CEBs inside;  $\lambda=260\ \mu\text{m}$ ; b) Schematic view of the array of CEBs, optimized for OLIMPO requirements. The array is placed on a silicon substrate of  $127\ \mu\text{m}$  thick. The CEB array consists of 96 dipole double-polarization antennas, each with two cold-electron bolometers; so the total number of CEBs is 192. Schematics of the experiment.

The total absorbed power is calculated as a sum of powers absorbed by each dipole antenna individually in the required frequency band around 345 GHz. We calculated absorbed power for different horn modes and obtained reasonably good results ( $43 \pm 3\%$ ) for the absorption efficiency.

## 3. Results

The electron temperature as well as accepted power are calculated by fitting of the experimental IV-curves. The fitting procedure is described in [21], that allows to calculate the accepted power with the precision of order  $0.2\text{pW}$ . The black body source (that can be heated up to 46K, keeping plate temperature at 0.3K) is placed inside the cryostat as shown in [21]. The measured CEB array demonstrates very effective electron cooling from 310 mK to 100 mK without optical power load,  $P_0$ , and from 330 mK to 160 mK with  $P_0=20\ \text{pW}$  at 345 GHz (Fig. 3). That means that even under high power load the CEBs are working at electron temperature less than the phonon temperature.

Dependences of cooling power,  $P_{cool}$ , electron-phonon power,  $P_{e-ph}$ , and absorbed power,  $P_0$ , obtained from two heat-balance equations [20] are shown in Fig. 4.

Horizontal lines show the phonon temperature, which is higher in case of incoming power due to microwave heating of the substrate. For  $P_0=0$  (Fig. 4a), when we increase voltage  $V$  and decrease  $T_e$ ,  $P_{e-ph}$  from phonons to electrons is increased and proportionally  $P_{cool}$  is increased to consume this heat flow:  $P_{e-ph} = \sum N (T_e^5 - T_{ph}^5)$ ,  $\sum$  is the material constant,  $N$  is the absorber volume. For  $P_0=20\ \text{pW}$  (Fig. 4b) at zero  $V$ , the total signal power  $P_0$  goes to phonons and  $P_{e-ph}$  has negative sign. Then, when we start to

increase  $V$  and decrease  $T_e$ ,  $P_{e-ph}$  is increased and crossed zero at critical point around  $V=3.8$  mV where cooling makes  $T_e$  lower than  $T_{ph}$ . For voltages higher than 3.8 mV  $P_{e-ph}$  is increased and proportionally  $P_{cool}$  is increased keeping difference between them equal to  $P_0$ .

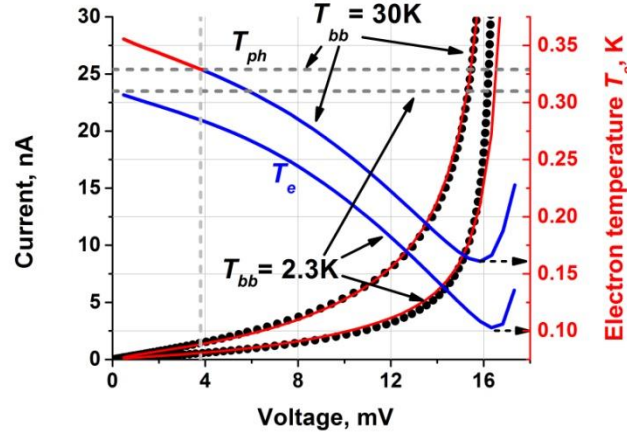


Fig. 3. IV-curves (black dots and solid red line) and dependences of electron temperature  $T_e$  (blue curves) on voltage for low power load  $P_0 = 0$  pW ( $T_{bb} = 2.3$  K) and high power load  $P_0 = 20$  pW ( $T_{bb} = 30$  K). The horizontal dashed lines correspond to phonon temperature.

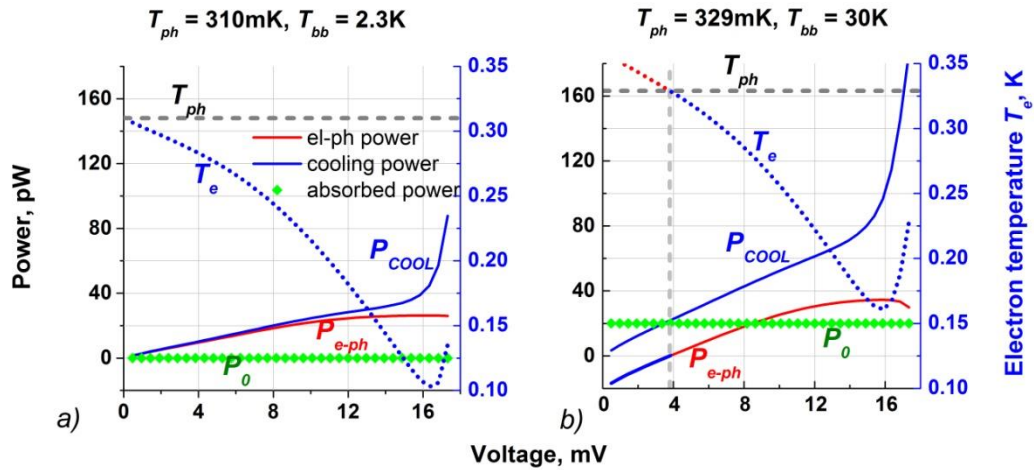


Fig. 4. a) Dependences of cooling power and e-ph power on voltage without optical power load,  $P_0=0$ ; electron temperature  $T_e$  is shown on the right; b) Dependences of cooling power and e-ph power on voltage with optical power load of  $T_{bb}=30$  K,  $P_0=20$  pW.

The electron-phonon thermal conductance,  $G_{e-ph}$ , and the cooling thermal conductance,  $G_{cool}$ , versus voltage for two different values of the incoming power are shown in Fig. 5a. Electron temperature is shown in Fig. 5b. Cooling conductance,  $G_{cool}$ , is increased with voltage and considerably overcomes  $G_{e-ph}$ . Both conductances are strongly increased for power load  $P_0=20$  pW. The strength of negative electrothermal feedback, the loop gain  $L$ , (green lines)

$$L = G_{cool}/G_{e-ph} \quad (1)$$

is increased for larger voltage and achieves a value of 10 without power load  $P_0$ , and a value of 100 for power load  $P_0=20$  pW.

Time response of the CEB ( $\tau$ ) versus voltage for two values of incoming power is shown in Fig. 5b.

$$\tau_{tot} = C_A / G_{tot} = \tau_{e-ph} (L + 1), \quad \text{with } G_{tot} = G_{cool} + G_{e-ph}, \quad (2)$$

Here  $C_A = A C_v$  - is the heat capacity of the normal metal;  $C_v = \gamma T_e$  is the specific heat capacity;  $A$  - the volume of the absorber and  $\tau_{e-ph}$  - the electron-phonon time constant.



As for TES [17], the time constant is strongly reduced by loop gain  $L$  (1) of the negative electrothermal feedback. Total time constant is mainly determined by cooling conductance  $G_{cool}$  dominated over  $G_{e-ph}$ . Maximum influence of electron cooling on time constant is for higher voltages where we have stronger cooling and lower  $T_e$  than for lower voltages.

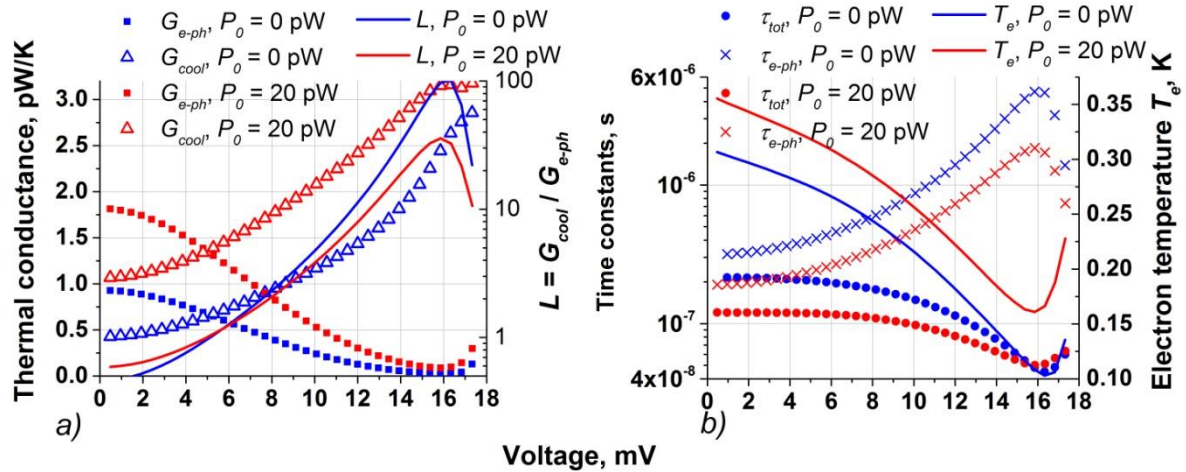


Fig. 5 a). Thermal conductance,  $G_{cool}$  and  $G_{e-ph}$ , for  $P_0=0$  (blue markers) and  $P_0=20$  pW (red markers) versus voltage of the CEB array. At the optimal operating point with minimum NEP,  $V=12$  mV,  $G_{cool}$  is considerably larger than  $G_{e-ph}$  and the difference is increased when optical power load is applied. The strength of negative electrothermal feedback, the loop gain  $L$  (solid curves), increases for larger  $P_0$  and achieves value of 10 at the optimal point.

Fig. 5b). Time constants,  $\tau_{tot}$  and  $\tau_{e-ph}$ , for  $P_0=0$  (blue markers) and  $P_0=20$  pW (red markers) versus voltage of the CEB array. The  $\tau$  is considerably shorter than  $\tau_{e-ph}$  due to short  $\tau_{cool}$ .

Various components of theoretically estimated voltage noise versus CEB array voltage are shown in Fig. 6 by solid curves, while the measured total voltage noise is shown by symbols with error marks.

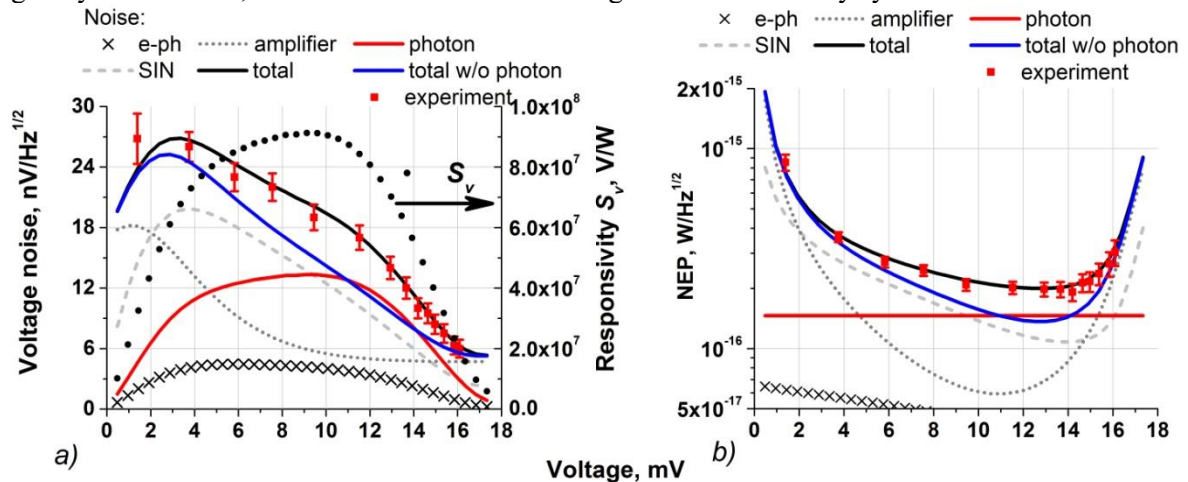


Fig. 6. Various components of voltage noise (a) and NEP (b) versus bolometer voltage. Curves - theory, red markers - experiment. Phonon temperature 330 mK, absorbed power 20 pW. Photon noise dominates over CEB noise from 11 to 14 mV.

Fig. 6 shows a good agreement between measured and theoretically estimated noise. In the voltage range, where photon noise exceeds the SIN and amplifier noise, one can see a small bump of the total noise at the voltages around (11-14) mV, which is well reproduced both in theory and experiment. We, therefore, can conclude that in this voltage range the photon noise dominates over the bolometer noise and is visible by the bolometer as in [20].

#### 4. Conclusion

The CEB with strong direct electron self-cooling of the nanoabsorber by SIN tunnel junctions have been realized for the 345 GHz channel of the OLIMPO balloon experiment. The ultimate photon-noise-limited operation of 2D array of CEBs is achieved due to effective electron self-cooling of the absorber. This cooling is acting as the strong negative electrothermal feedback improving noise and dynamic characteristics. The absorption in the required frequency band is realized thanks to the 2D array of dipole antennas on a thinned Si substrate. This operation was demonstrated with  $P_0$  in the range (10-20) pW at  $T_{ph}$  from 310 to 330 mK. This means that even under relatively high power load the CEBs are working at electron temperature  $T_e=160$  mK, i.e. much less than the phonon temperature. This is the first realization of the bolometer working at electron temperature colder than the phonon temperature under relatively high power load.

#### 5. Acknowledgements

We would like to thank Mikhail Tarasov for help in fabrication of samples and Dmitry Golubev and Vyacheslav Vdovin for useful discussions. The work was supported by the Swedish National Space Board, SNSB, and Russian Science Foundation (Project No. 16-19-10468). Samples were fabricated at the Chalmers Nanotechnology Center.

#### References

- [1] Cho A: Insights of the decade: precision cosmology. *Science* 2010, 330:1615.
- [2] Masi S, et al: Instrument, method, brightness and polarisation maps from the 2003 flight of BOOMERanG. *Astron Astrophys* 2006, 458:687–716. astro-ph/0507509.
- [3] S. Masi, E. Battistelli, D. Brienza et al., "OLIMPO", *Mem. S. It.*, vol. 79, p.887, 2008.
- [4] P. de Bernardis, S. Colafrancesco, G. D'Alessandro, L. Lamagna, P. Marchegiani, S. Masi and A. Schillaci, Low-resolution spectroscopy of the Sunyaev-Zel'dovich effect and estimates of cluster parameters, *Astronomy & Astrophysics*, A86, 538 (2012).
- [5] L. Kuzmin. "Optimization of the Hot-Electron Bolometer for Space Astronomy", *SNED Proc. Vol. 1*, pp. 145–154 (2002).
- [6] L. Kuzmin, "Ultimate Cold-Electron Bolometer with Strong Electrothermal Feedback", in *Proc. of the SPIE conference "Millimeters and Submillimeter Detectors"*, vol. 5498, pp. 349-36, 2004.
- [7] M. Salatino, P. de Bernardis, L.S. Kuzmin, S. Mahashabde, S. Masi, "Sensitivity to cosmic rays of cold electron bolometers for space applications", *J. Low Temp. Phys.*, vol. 176, p. 323, 2014.
- [8] M. L. Roukes, M. R. Freeman, R. S. Germain, and M.B. Ketchen, *Phys. Rev. Lett.* 55, 422 (1985).
- [9] M. Nahum, T. M. Eiles and J. M. Martinis, *Appl. Phys. Lett.* 65, 3123 (1994).
- [10] M. M. Leivo, J. P. Pekola, and D. V. Averin, *Appl. Phys. Lett.* 68, 1996 (1996).
- [11] L. Kuzmin, I. Agulo, M. Fominsky, A. Savin, and M. Tarasov. Optimization of the electron cooling by SIN tunnel junctions. *Supercon. Sci. Technol.*, 17, S400 (2004).
- [12] A. J. Manninen, M. M. Leivo, and J. P. Pekola Refrigeration of a dielectric membrane by SINIS tunneling. *Appl. Phys. Lett.* 70, 1885 (1997);
- [13] N. A. Miller, G. C. O'Neil, J. A. Beall, G. C. Hilton, K. D. Irwin, D. R. Schmidt, L. R. Vale, and J. N. Ullom, *Appl. Phys. Lett.* 92, 163501 (2008).
- [14] N. Vercruyssen, R. Barends, T. M. Klapwijk, J. T. Muhonen, M. Meschke, and J. P. Pekola, *Appl. Phys. Lett.* 99, 062509 (2011).
- [15] H. Q. Nguyen, M. Meschke, and J. P. Pekola, A robust platform cooled by superconducting electronic refrigerators, *Applied Physics Letters* 106, 012601 (2015).
- [16] L. Kuzmin and D. Golubev "On the concept of an optimal hot-electron bolometer with NIS tunnel junctions". *Physica C* 372-376, 378-382 (2002).
- [17] K. Irwin. *Applied Physics Letters* 66, 1998 (1995).
- [18] L. Kuzmin, "2D Array of Cold-Electron Nanobolometers with Double Polarization Cross-Dipole Antennae", *Nanoscale Research Lett.*, 7:224 (2012).
- [19] L. Kuzmin and A. Sobolev. "Wideband Double-Polarized Array of Cold-Electron Bolometers for OLIMPO Balloon Telescope", to be submitted to *Nature Scientific Reports* (December 2017).
- [20] L. Kuzmin, "An array of cold-electron bolometers with SIN tunnel junctions and JFET readout for cosmology instruments," in *Journal of Physics: Conference Series*, vol. 97, 2008, p. 012310
- [21] A.V. Gordeeva, et al., "Observation of photon noise by cold-electron bolometers", *Appl. Phys. Lett.*, 110, 162603 (2017).